iScience

CellPress
OPEN ACCESS

Article

Characterizing the extracellular vesicle proteomic landscape of the human airway using *in vitro* organotypic multi-cellular models

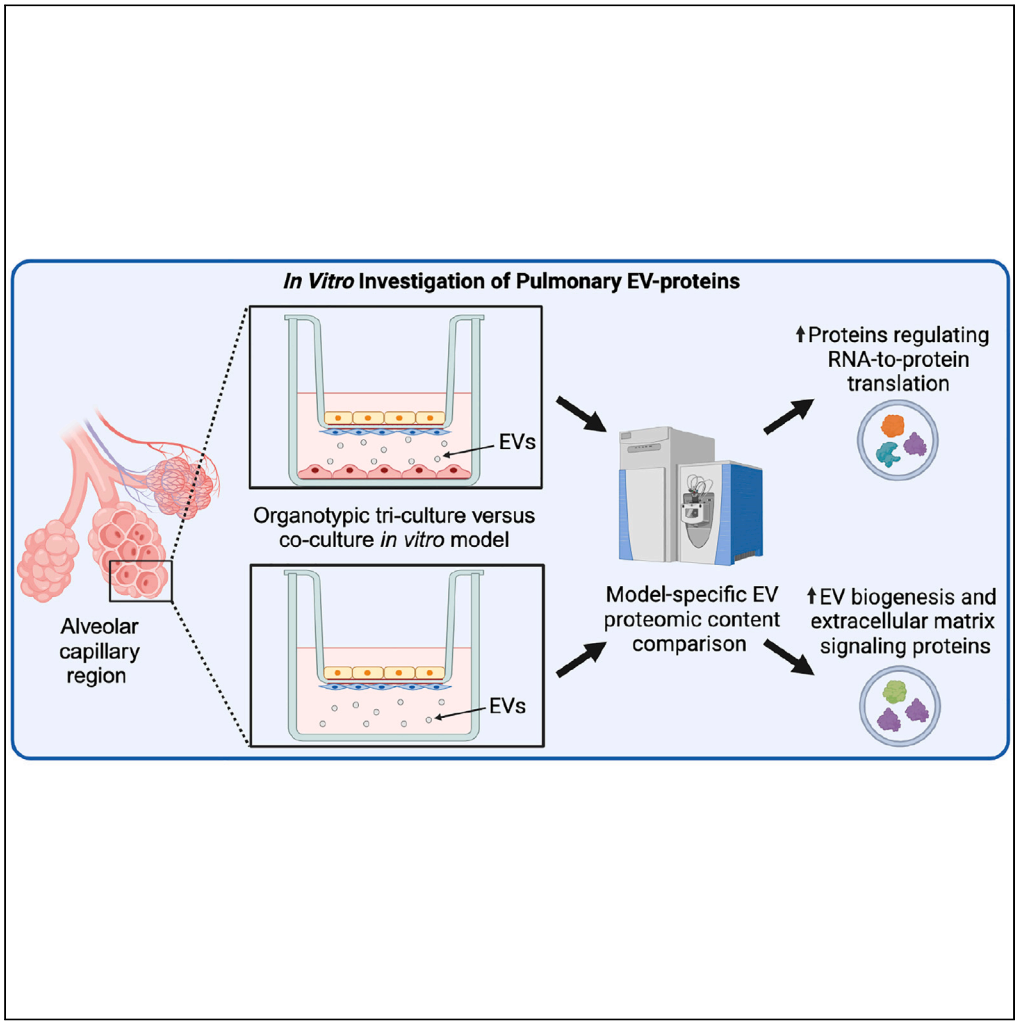

Eva C.M. Vitucci, Celeste K. Carberry, Alexis Payton, Laura E. Herring, Angie L. Mordant, Shaun D. McCullough, Julia E. Rager

smccullough@rti.org (S.D.M.)
jrager@unc.edu (J.E.R.)

Highlights

Organotypic airway models can investigate EV-mediated intercellular communication

Increasing *in vitro* model complexity alters EV proteomic content and diversity

Different pulmonary cell types uniquely affect EV proteomic composition

Cellular composition of *in vitro* models is important to consider in EV studies

Vitucci et al., iScience *26*, 108162
November 17, 2023
https://doi.org/10.1016/j.isci.2023.108162

iScience

CellPress
OPEN ACCESS

Article

Characterizing the extracellular vesicle proteomic landscape of the human airway using *in vitro* organotypic multi-cellular models

Eva C.M. Vitucci,[1,2,3] Celeste K. Carberry,[4,5] Alexis Payton,[3,4] Laura E. Herring,[6] Angie L. Mordant,[6] Shaun D. McCullough,[2,7,8,*] and Julia E. Rager[2,3,4,5,9,*]

SUMMARY

Extracellular vesicle (EV)-mediated intercellular communication significantly influences pulmonary cell health and disease, yet *in vitro* methods to investigate these mechanisms are limited. We hypothesize that organotypic models of the airway can be leveraged to investigate EV-mediated intercellular signaling, focusing on EV proteomic content as a case study. Two *in vitro* airway culture models were evaluated by mass spectrometry-based proteomics analysis: a tri-culture model consisting of alveolar epithelial, fibroblast, and lung microvascular endothelial cells and a co-culture model of alveolar epithelial and fibroblasts. EVs isolated from the tri-culture model were enriched with EV proteins regulating RNA-to-protein translation. EVs isolated from the co-culture model were enriched with EV biogenesis and extracellular matrix signaling proteins. These model-specific differences suggest that different pulmonary cell types uniquely affect EV composition and the biological pathways influenced by the EV proteome in recipient cells. These findings can inform future studies surrounding EV-related pulmonary disease pathogenesis and therapeutics.

INTRODUCTION

Extracellular vesicles (EVs) are small, membrane-bound particles released by a cell into the extracellular space.[1–4] EVs can contain nucleic acids, proteins, and lipids from their cell of origin and can release this cargo into a recipient cell upon fusion with the cell membrane.[1–4] This transfer of EV cargo can significantly alter gene and protein expression in the recipient cell, thereby altering biological signaling pathways and inducing functional changes.[5] Consequently, EVs are key mediators of intercellular communication that can contribute to the physiological maintenance of a tissue and disease pathogenesis.[1–7]

EVs are of broad interest because of their association with a variety of pathologies, including the progression of several pulmonary diseases.[4,5,8–11] Indeed, pulmonary EVs have pathophysiological roles in acute respiratory distress syndrome (ARDS), chronic obstructive pulmonary disease (COPD), interstitial pulmonary fibrosis (IPF), and multiple other lung diseases.[4,8–17] Pulmonary EVs are also of broad interest because of their potential to serve as novel therapeutic delivery vesicles to the pulmonary tissue.[18] Despite the high biological significance of pulmonary EVs, questions remain regarding EV biogenesis, how EV cargo directs intercellular communication, and how specific cell types of the airway modulate these processes.

Currently, there is a paucity of *in vitro* methods available to evaluate these EV processes in the airway.[12,19] Recent studies comparing *in vitro* monocultures to organotypic cultures of cancer cell lines found EV composition from organotypic models more closely corresponds with EV composition derived from patient plasma samples.[20–22] Thus, *in vitro*, organotypic models may significantly improve our understanding of *in vivo* EV-mediated intercellular signaling.

In terms of the pulmonary system, EVs secreted from the alveolar capillary region (ACR) play significant roles in mediating pulmonary homeostasis and disease pathogenesis.[4,10] The ACR is a large, susceptible, and influential region of the lung, coincidently involved in the pathogenesis of many respiratory diseases, such as ARDS, COPD, and IPF.[4,16,23,24] The ACR represents the interface of the respiratory and cardiovascular system and is composed of multiple cell types. Notably, the resident alveolar epithelial, interstitial fibroblasts, and

[1]Interdisciplinary Faculty of Toxicology, School of Public Health, Texas A&M University, College Station, TX, USA
[2]Curriculum in Toxicology & Environmental Medicine, School of Medicine, University of North Carolina, Chapel Hill, NC, USA
[3]The Center for Environmental Medicine, Asthma and Lung Biology, School of Medicine, The University of North Carolina, Chapel Hill, NC, USA
[4]Department of Environmental Sciences and Engineering, Gillings School of Global Public Health, The University of North Carolina at Chapel Hill, Chapel Hill, NC, USA
[5]The Institute for Environmental Health Solutions, Gillings School of Global Public Health, The University of North Carolina at Chapel Hill, Chapel Hill, NC, USA
[6]UNC Proteomics Core Facility, Department of Pharmacology, The University of North Carolina at Chapel Hill, Chapel Hill, NC, USA
[7]Public Health and Integrated Toxicology Division, Center for Public Health and Environmental Assessment, U.S. Environmental Protection Agency, Chapel Hill, NC, USA
[8]Exposure and Protection, RTI International, Durham, NC, USA
[9]Lead contact
*Correspondence: smccullough@rti.org (S.D.M.), jrager@unc.edu (J.E.R.)
https://doi.org/10.1016/j.isci.2023.108162

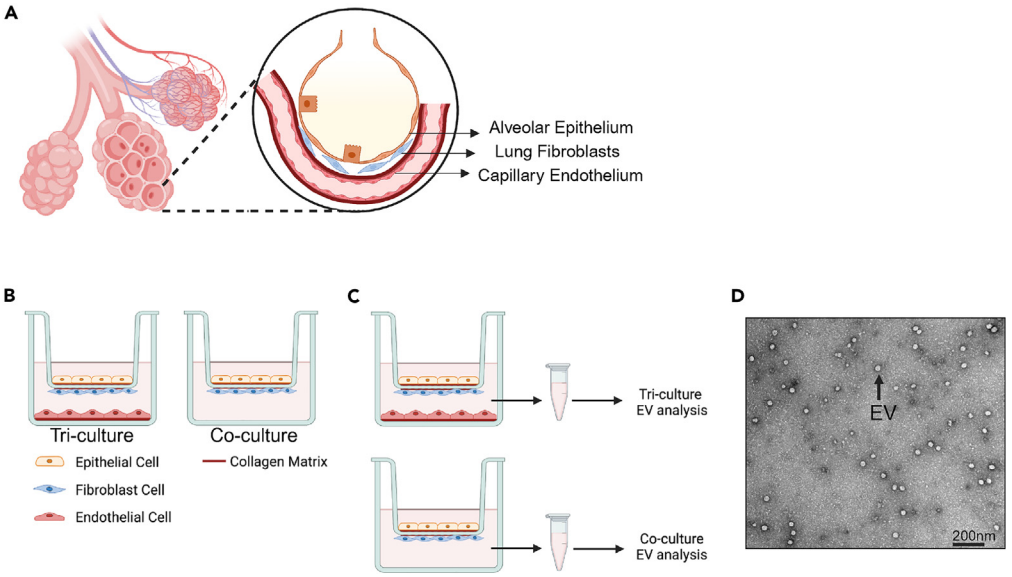

Figure 1. Overview of the *in vitro* organotypic models and EV isolation

(A) Representation of the alveolar capillary region *in vivo*.

(B) Schematics of the tri- and co-culture models of the airway are shown.

(C) EVs were isolated from the basolateral conditioned medium from both models to inform potential intercellular communication occurring through EV proteomic expression signatures.

(D) A representative transmission electron micrograph of EVs isolated from basolateral conditioned medium of the tri- and co-culture models (an image from the tri-culture model is specifically shown here). EVs are shown as white circles, with an example EV indicated by a black arrow. A 200 nm scale bar is displayed in the bottom right corner.

microvascular endothelial cells play key roles in maintaining homeostasis in the ACR and in disease progression.[4] The alveolar epithelium lines the alveolar air sacs and provides an extensive surface area for gas exchange while also forming a tight, physical barrier that prevents inhaled substances from entering the cardiovascular system. In addition, the microvascular endothelium lines the dense vascular network surrounding the alveoli. The endothelium also contributes to gas exchange and, in conjunction with the interstitial fibroblasts, the regulation of pulmonary immune cell trafficking.[25,26] Consequently, alterations in epithelial and endothelial signaling, as well as in the interstitial fibroblasts that bridge these cell types *in vivo*, can have direct impacts on both the respiratory and cardiovascular systems.

Here, we test the hypothesis that organotypic models of the ACR can be leveraged to investigate how cells of the ACR mediate intercellular communication through the EV proteome. Utilizing mass spectrometry-based proteomics, we compared the EV proteome between two organotypic models of the ACR: (1) a tri-culture model consisting of alveolar epithelial, lung fibroblasts, and lung microvascular endothelial cells and (2) a co-culture model consisting of alveolar epithelial and lung fibroblasts to evaluate EVs in the absence of endothelial cells. Proteomics analysis highlighted differences in EV protein content between the models, as well as related biological pathways. These model-specific differences in EV proteomic content suggest that specific pulmonary cell types have unique effects on EV composition and subsequent EV-mediated intercellular communication. These differences highlight the utility of organotypic models in investigating cell type-specific mechanisms to improve our understanding of EV-mediated intercellular signaling and the development of future EV-based therapeutic approaches.

RESULTS

Overview of tri-culture and co-culture models

3D organotypic tri-culture and co-culture models of the ACR were used in this study to evaluate culture model-specific contributions to EV release and associated proteomic content (Figure 1, Table 1). Here, the tri-culture model was implemented to evaluate EV-associated communication mechanisms between alveolar epithelial cells (H441) and lung fibroblasts (IMR90) seeded on opposite sides of a Transwell insert, and microvascular endothelial cells (HULEC) seeded in the basolateral compartment of a Transwell well. A simplified co-culture model was also used to evaluate EVs in the absence of endothelial cells.

Cell viability and small molecule permeability measures

Cell viability and small molecule permeability were evaluated in the tri- and co-culture models after 24 h. There were no significant changes in cell viability across the tri- and co-culture models (Figures S1A and S1B). In terms of small molecule permeability, permeability of both the

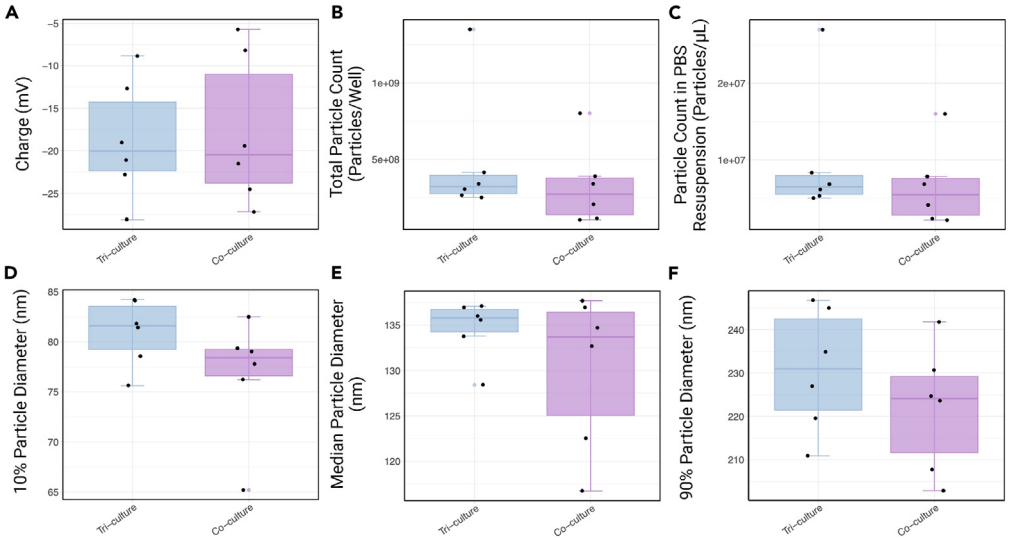

Figure 2. Physical characteristics of EV samples, as measured through Nanoparticle Tracking Analysis (NTA)

EV physical measures included (A) particle charge; (B) particle count converted into concentration values from the 12-well format *in vitro* models' conditioned media; (C) particle count within the analyzed sample resuspended in PBS; (D) average 10% particle diameter; (E) average 50% (i.e., median) particle diameter; and (F) average 90% particle diameter. Data are displayed as bar charts, with the median marked as a solid line in the middle, and the bars expanding across the 25% and 75% data distributions. Individual black dots represent the actual measured values. Note that none of these physical measures differed significantly between groups.

0.4 kDa fluorescein isothiocyanate (FITC) molecule and the 4 kDa tetramethylrhodamine isothiocyanate (TRITC)-dextran molecule across the seeded Transwell insert of the tri- and co-culture models spanned between an average of 1% and 4% permeability, as compared to 100% permeability of the insert alone (Figures S1C and S1D). Low permeability of small-molecular-weight compounds across epithelial layers, such as that observed here, is indicative of an established alveolar epithelial barrier.[27]

Physical characteristics of EVs isolated from conditioned media

Microscopy imaging and nanoparticle tracking analysis (NTA) were carried out to assess the physical characteristics of EVs isolated from the basolateral conditioned medium. Microscopy results showed that the basolateral conditioned medium samples were enriched for EVs, indicated by circular particles with diameters largely <100 nm (Figures 1D and S4). NTA measured particle charges averaging −18.7 and −17.8 mV for the tri- and co-culture models, respectively (Figure 2A). These charges are within range of previously reported values of EVs derived from *in vitro* conditioned media samples.[28–30] Particle counts indicated EV concentration averages of 9.75 x 10^6 and 6.52 x 10^6 particles/µL PBS in the tri- and co-culture model samples, respectively (Figure 2B). These concentrations equated to total particle counts of 4.88 x 10^8 and 3.26 x 10^8 particles per well of basolateral conditioned medium in the tri- and co-culture model, respectively, plated in the 12-well format (Figure 2C). Particle sizes measured via NTA averaged across all samples were as follows: 10% particle diameter of 78.8 nm, median particle diameter of 132.4 nm, and 90% particle diameter of 226.3 nm (Figures 2D–2F). Size deviation between NTA and microscopy methods have previously been characterized and are hypothesized to be attributable to shrinkage resulting from transmission electron microscopy sample preparation, as well as size distortion due to resolution limits of NTA.[31] While there are notable differences between the average EV size illustrated in the microscopy image, acquired from one part of a sample, and NTA measures, acquired from larger subsets of many samples, both distributions overlap with those typically reported for the EV subtype of small EVs (largely <200nm).[1] No particle characteristics were significantly different between culture models (Table S1).

EV proteomic landscape in tri- and co-culture models

Proteomic analysis identified 1,336 unique proteins; 1,270 of which were detected in the tri-culture model and 905 in the co-culture model (Table S2). Of these, 431 proteins were only found in the tri-culture and 66 proteins were only found in the co-culture EVs. The remaining 839 proteins were detected in EVs isolated from both *in vitro* models (Figure 3A).

To investigate how the additional cell type in the tri-culture model, the microvascular endothelial cells, affected EV proteomic content, we statistically compared the abundances of EV proteins detected in the tri-culture model to those in the co-culture model. Of the 839 proteins detected in both models, 469 were identified as significantly, differentially ($p_{adj} < 0.05$ and $\log_2$ fold change [FC] $\geq +/- 0.585$) loaded into EVs when comparing the tri-culture model vs. co-culture model samples, 431 of which were increased in the tri-culture model and 38 were increased in the co-culture model. The remaining 370 proteins that were detected across both models were not significantly, differentially loaded into EVs from either model (Figures 3A and 3B). The 431 and 66 proteins detected in only the tri- and co-culture models, respectively,

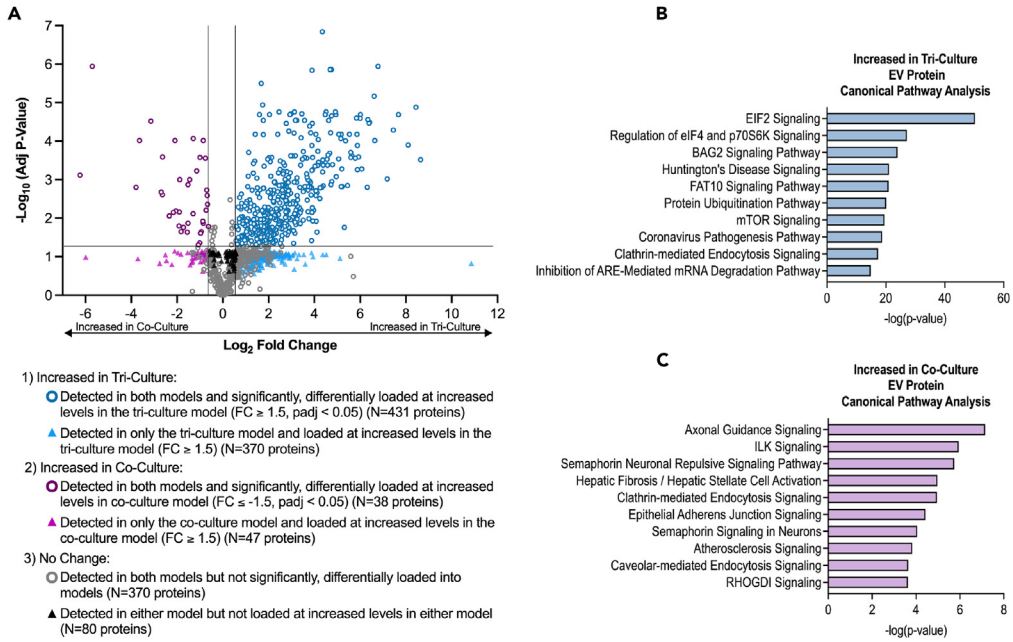

Figure 3. Comparative proteomic landscape of EVs isolated from conditioned media of 3D organotypic tri- and co-culture models of the airway epithelium

(A) Volcano plot of tri-culture and co-culture EV proteins and their designation into summary-level protein lists. Proteins are colored and shape dependent according to their detection across the culture models and their level of significant, differential expression in tri-culture vs. co-culture samples. Note that some proteins were only detected in one of the models and did not reach the strict statistical threshold for significance as a result of comparison against non-detected proteins. These proteins are displayed with different shapes than proteins meeting statistical significance (see legend).

(B) The top 10 most significant pathways associated with the EV proteins increased in the tri-culture model (represented by the blue proteins in panel A).

(C) The top 10 most significant pathways associated with EV proteins increased in the co-culture model (represented by the purple proteins in panel A). For all pathways, see Table S3.

did not reach statistical significance when comparing abundance distributions between the tri- and co-culture models, likely due to a strict multiple test corrected p value filter requirement that could not be obtained when including values below detection limits. However, 370 and 47 EV proteins found only in the tri- and co-culture models, respectively, were considered differentially loaded based on an FC criterion of $\geq \pm 1.5$ (Figures 3A and 3B). To generate summary-level protein lists to carry forward in analyses and biological interpretations, we established the following three groups of detected EV proteins: (1) "Increased in tri-culture" (n = 801 proteins with $\log_2FC \geq 0.585$ [tri-culture/co-culture], 431 of which reached $p_{adj} < 0.05$); (2) "Increased in co-culture" (n = 85 proteins with $\log_2FC \leq -0.585$ [tri-culture/co-culture], 38 of which reached $p_{adj} < 0.05$); and (3) "No change" (n = 450 proteins).

Alignment of EV proteomic landscape with markers of EV presence and purity

A large number (n = 22) of detected proteins overlapped with the International Society for Extracellular Vesicles (ISEV) Minimal Information for Studies of Extracellular Vesicles (MISEV)'s list of established protein markers of EV presence and purity (Table S2).[32] To detail, 14 proteins belonged to the "class 1" category spanning transmembrane or glycophospholipid (GPI)-anchored proteins that inform the presence of an EV lipid bilayer, including the following: Disintegrin and metalloproteinase domain-containing protein 10 (ADAM10), Amyloid-beta precursor protein (APP), Basigin (BSG), several cluster of differentiation (CD) molecules (e.g., CD55, CD59, CD63, CD81, and CD9), Epithelial cell adhesion molecule (EPCAM), several human leukocyte antigen (HLA) class I histocompatibility antigens (e.g., HLA-A, HLA-B, and HLA-C), 5′-nucleotidase (NT5E), and Platelet endothelial cell adhesion molecule (PECAM1). Seven proteins belonged to the "class 2" category of cytosolic proteins present in eukaryotic cells that commonly incorporate into EVs, including Glyceraldehyde-3-phosphate dehydrogenase (GAPDH), Heat shock protein HSP 90-beta (HSP90AB1), and Heat shock cognate 71 kDa protein (HSPA8), among others. One protein belonged to the "class 3" category of proteins that often co-isolate with EVs and are thus considered contaminants, namely Apolipoprotein B-100 (APOB). These findings support the successful isolation and proteomic evaluation of EV proteins from these *in vitro* models.

Pathway and cellular component-level changes between culture models

To better understand the potential biological functions and related cellular locations of the detected EV proteomes, canonical pathway and cellular component enrichment analyses were carried out. Analyses were organized by separating the proteins into the following bins: (1)

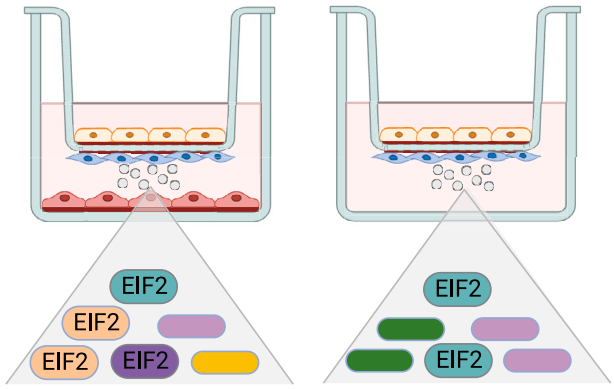

Figure 4. Summary of EV proteomic similarities and differences across *in vitro* culture models

Overall, the number and size distribution of EVs released across both models were similar, but the diversity of protein molecules was considerably increased in the tri-culture vs. co-culture model. Furthermore, the tri-culture model showed greater enrichment for EIF2 and RNA translation pathway-level processes.

"Increased in tri-culture" (n = 801 proteins); (2) "Increased in co-culture" (n = 85 proteins); and (3) "No change" (n = 450 proteins), as described in the aforementioned results and illustrated in Figure 3.

Pathway enrichment analyses found approximately 3x as many signaling pathways enriched among the EV proteins in the "Increased in tri-culture" compared to those in the "Increased in co-culture" groups (Table S3A), paralleling the larger diversity of proteins detected in the tri-culture model vs. co-culture model. Many of the most significantly detected pathways in the "Increased in tri-culture" group were associated with the regulation of mRNA translation. Notably, the most significant pathway associated with the EVs within the "Increased in tri-culture" group was the "eukaryotic initiation factor 2 (EIF2) signaling" pathway ($p = 6.31x10^{-51}$) with 74 proteins involved in EIF2 signaling detected (Figure 3C). The top canonical signaling pathways associated with the EV proteins in the "Increased in co-culture" group were related to axonal guidance signaling and endocytosis (Table S3B). The most significant pathway of this group was the "axonal guidance signaling" pathway ($p = 7.08x10^{-8}$) with 13 proteins involved in signaling detected (Figure 3C). The EIF2 signaling pathway was also the most significant pathway associated with the EV proteins within the "No change" group, with 27 proteins involved in EIF2 signaling detected ($p = 2x10^{-11}$) (Table S3C).

Cellular component enrichment analysis results largely aligned with the pathway analysis results for each group. The cellular component analysis revealed EV proteins within the "Increased in tri-culture" group were significantly enriched with proteins affiliated with mRNA translation complexes such as the aminoacyl-tRNA synthetase multienzyme complex (fold enrichment = 25.05, $p = 1.89x10^{-7}$) and the eukaryotic translation initiation factor 3 (EIF3) complex (fold enrichment = 25.05, $p = 5.14x10^{-4}$), among others (Table S4A). In addition, the cellular component analysis revealed EV proteins within the "Increased in co-culture" group were significantly enriched with proteins affiliated with complexes such as the "protein complex involved in cell-matrix adhesion" (fold enrichment = 66.1, $p = 1.48x10^{-3}$) and the "basement membrane" (fold enrichment = 20.61, $p = 1.72x10^{-6}$), among others (Table S4B). EV proteins within the "No change" group were significantly enriched with proteins associated with the beta-subunit of the "proteasome complex" (fold enrichment = 24.36, $p = 1.70x10^{-3}$) (Table S4C). EV proteomic enrichment similarities and differences between culture models are additionally summarized in Figure 4.

Protein-specific validation of EV isolates

The EV proteomics screen detected 59 EV proteins that overlap with the MISEV category 1–3 proteins between both culture models (Table S2). ALIX (PDCD6IP), ANXA5, CD63, CD81, and EpCAM are 6 of these EV protein markers (Figure S2). Two of these proteins (i.e., ALIX and ANXA5) also overlap with the MISEV category 1 proteins, as previously described. EV protein markers were then validated among a representative sample of EV isolates from the tri-culture model using a pre-loaded antibody array of proteins commonly evaluated in EV studies. The following proteins were measured within this sample: ANXA5, ICAM, CD63, ALIX, CD81, TSG101, FLOT1, and GM130 (Figure S3). Notably, some additional proteins were detected via the exocheck antibody array, which were not detected via proteomics (e.g., TSG101, FLOT1, and GM130). Together, these findings support the successful isolation of EVs and their associated protein content from cell culture media.

DISCUSSION

This study aimed to leverage *in vitro* models of the airway, specifically of the ACR, to further our understanding of EV-mediated intercellular signaling mechanisms across specific combinations of pulmonary cell types. Two different organotypic models of the ACR were evaluated: a

Table 1. Experimental design for the establishment and application of the tri- and co-culture models

Components	6-well (24 mm insert) Corning #3450	12-well (12 mm insert) Corning #3460
Downstream Application	EV Proteomics [6 biological replicates per condition, 4 technical replicates combined due to sample yield requirements]	Cell Viability [3 biological replicates per condition], Small Molecule Permeability Assays [6 biological replicates per condition], EV Microscopy [subset of 2 samples], EV NTA [6 biological replicates per condition]
Insert (Apical Compartment) Growth Area	4.67 cm^2	1.12 cm^2
Well (Basolateral Compartment) Growth Area	9.5 cm^2	3.8 cm^2
Apical Media Volume	2000 µL	500 µL
Basolateral Media Volume	2000 µL	1000 µL
Inverted Plating Volume	1000 µL	250 µL
Diluted H441 Cell Suspension	1.75×10^5 cells/mL	16.8×10^4 cells/mL
H441 Cell Density	7.5×10^4 cells/cm^2	7.5×10^4 cells/cm^2
H441 Cell Count	3.5×10^5 cells/insert	8.4×10^4 cells/insert
Diluted IMR90 Cell Suspension	2.9×10^4 cells/mL	2.8×10^4 cells/mL
IMR90 Cell Density	6.25×10^3/cm^2	6.25×10^3/cm^2
IMR90 Cell Count	29,000 cells/insert	7,000 cells/insert
Diluted HULEC Cell Suspension	1.38×10^5 cells/mL	1.12×10^5 cells/mL
HULEC Cell Density	2.9×10^4 cells/cm^2	2.9×10^4 cells/cm^2
HULEC Cell Count	275,500 cells/B.C.	112,000 cells/B.C.
Downstream EV Sample Resuspension Volume in Filtered PBS	200 µL	50 µL

Tri- and co-culture models were established using 6-well or 12-well formats, depending on the indicated downstream application. The number of experimental replicates conducted for each application is specified in brackets. Basolateral compartment, B.C.

tri-culture model consisting of alveolar epithelial, fibroblast, and lung microvascular endothelial cells, and a co-culture model consisting of alveolar epithelial cells and lung fibroblasts seeded in separate compartments across a Transwell insert. Notably, the implemented alveolar epithelial and microvascular endothelial cell lines reflect multiple important features of the ACR *in vivo* such as alveolar epithelial barrier formation and surfactant protein production[33,34] and are representative of the epithelial and microvascular endothelial cells found in the human ACR. Comparing EVs secreted from the tri- and co-culture *in vitro* airway model revealed that EV physical characteristics, including particle number and size distribution, remained consistent between the two models. When evaluating EV proteomic signatures, however, the following differences were apparent: (1) there was greater diversity in the proteins detected in the tri-culture model (n = 1,270 proteins) vs. co-culture model (n = 905 proteins) and (2) the biological pathways associated with EV proteins were differentially enriched in the tri-culture vs. co-culture models. These model-specific differences in EV proteomic content suggest that specific pulmonary cell types may have unique effects on EV-mediated intercellular communication.

Proteins within EVs are becoming increasingly recognized as important contributors of EV-mediated intercellular communication.[10,19,35–38] Here we show an increased diversity of proteins in EVs isolated from the tri-culture compared to the co-culture model of the airway epithelium. Our observations demonstrate that increasing the biological complexity (i.e., incorporating an additional *in vivo*-relevant cell type) of an *in vitro* model can alter the EV proteome of the system, thus, highlighting the importance of considering the cellular composition of *in vitro* systems used in EV studies, especially in the context of identifying potential biomarkers of exposure and/or disease. Future studies are needed to identify the relative contributions of different cell types and their potential to influence intercellular communication.

Characterization of the proteins identified at increased levels in tri-culture EVs (vs. co-culture EVs) revealed an enrichment in RNA binding proteins such as multiple eukaryotic translation initiation factors, ribosomal proteins, and protein chaperones. These proteins are significantly associated with cellular components involved in protein translation such as the Aminoacyl-tRNA Synthetase Multienzyme and the EIF3 complexes.[39] Accordingly, these proteins are also associated with signaling pathways involved in the regulation of protein translation, such as the EIF2 signaling pathways. Many of the significantly enriched pathways associated with the altered tri-culture EV proteins, including EIF2 signaling, can be activated by a diverse array of stress-related signals that direct global and specific mRNA translation.[40–43] However, findings from the current analysis demonstrate increased detection of EIF2 signaling-related proteins in the absence of an applied exogenous stressor or overt cell stress, as evidenced by a lack of cytotoxicity in the culture models and maintenance of normal cellular morphology. Our observations reported here parallel previous studies that have identified a similar enrichment for proteins involved in EIF signaling and translation

across EV proteomes from various cell types, in the absence of cellular stress.[44–46] This persistent detection of RNA binding proteins in EVs may suggest either an active or passive role of these proteins in the RNA loading of EVs in the donor cell. Future studies investigating this putative role may help elucidate important mechanisms of EV biogenesis. Furthermore, as EV content can be released into the recipient cell cytoplasm, the transfer of translational machinery could also significantly enhance the translation of transferred EV cargo that acts through RNA-to-protein translational mechanisms and increase the efficacy of EV-mediated intercellular signaling. Indeed, the investigation of EV proteins that increase the delivery of EV therapeutic cargo into target cells and its efficacy is of growing interest.[30,45,47] Ovchinnikova et al.[45] suggest the incorporation of protein chaperones into EVs designed for drug delivery may help stabilize the structure of therapeutic proteins within the EV and improve the therapeutic efficacy upon delivery. With the recent advancement of mRNA packaging into EVs,[47–51] our observations build upon those reported by Ovchinnikova et al.[45] and support the value of future studies to investigate whether co-packaging of translational machinery with mRNA therapeutic molecules may enhance the mRNA translation and therapeutic effect upon delivery.

EV packaging of proteins involved in translational machinery increased with the addition of the endothelial cells in the tri-culture model. The airway has the highest vascular density in the human body; therefore, it is plausible that endothelial EV signaling would have influential effects on airway homeostasis and disease development.[52] Endothelial cells and endothelial-derived EVs and microparticles are associated with the pathogenesis of a number of pulmonary diseases.[53–55] The tri-culture model of the airway described herein may therefore be a useful tool to identify causative mechanisms of endothelial EV-mediated intercellular communication in airway disease development. Furthermore, this model may also be a useful tool to identify candidate biomarkers of toxicant exposure and/or pulmonary disease involving the pulmonary microvasculature vasculature.[56,57]

In the absence of endothelial cells, EV proteins at increased levels in the co-culture model were associated with fewer biological pathways compared to the tri-culture EV proteins. Of the pathways associated with these EV proteins, the most significant pathway was the "Axonal Guidance" signaling pathway. A large number of metalloproteases and integrins contributed to the classification of this pathway as being alternatively regulated. A growing number of studies have also detected metalloproteases and integrins in EVs.[58–63] Metalloproteases are thought to contribute to EV biogenesis, modification, and EV uptake by recipient cells through the remodeling of the extracellular matrix (ECM) and the modification of EV and cell surface receptors.[62,63] Furthermore, EV-bound integrins are involved in adhesion to the ECM and EV uptake by recipient cells.[60,61] While studies have shown these proteins' involvement in EV biogenesis, migration through the ECM, and the homing of EVs to specific cell types in disease states such as cancer and kidney disease, these mechanisms and/or resulting biological consequences in the airway are still relatively unclear.[61,64] The enrichment of these proteins and associated signaling pathways in the co-culture EVs suggest metalloproteases and integrins likely mediate these processes in the airway as well. Thus, our results suggest the co-culture model described herein may be a valuable tool to investigate the mechanisms of EV biogenesis, migration, and recipient cell uptake in the airway.

It is becoming increasingly evident that EVs and their cargo are mediators of airway health and disease. Here, we observed that the cellular complexity of organotypic models affects the proteomic cargo of secreted EVs, which may have significant implications for future investigation of mechanisms involved in intercellular communication within the pulmonary airways. Thus, increasing the representation of different *in vivo*-relevant cell types into *in vitro* organotypic models can improve our ability to investigate the different aspects of EV-mediated signaling mechanisms and to develop EV-based interventions for respiratory disease. Further work using organotypic models of the airway is needed to continue advancing our mechanistic understanding of EV communication in the airway and its role in maintaining lung homeostasis and disease development.

Limitations of the study

Our study has identified significantly enriched signaling pathways in the tri- and co-culture EVs after 24 h in culture; however, we did not investigate EV proteomics at other time points. Future studies are needed to investigate if culture time modulates EV proteins and affiliated signaling pathways. We also did not exclusively investigate the cell type of origin of the EVs detected in the culture models, and how this contributes to the diversity of the detected EV proteome. Future investigations can build upon this work and provide further insight into cell-specific roles in EV-mediated intercellular communication in the lung. The cellular composition of our *in vitro* models represents the ACR of the lung; therefore, our findings may more closely reflect EV signaling from the respiratory region of the respiratory system. Future studies using *in vitro* models of the conducting (i.e., tracheobronchial) region are needed to investigate how EV signaling may differ throughout the respiratory tract. Lastly, while the incorporated human cell lines were all immortalized from pulmonary tissue and, unlike other alveolar-like epithelial cell lines, exhibit the crucial epithelial barrier function of the ACR, our models do not incorporate primary cell types. Thus, future studies could better address inter-individual response variability in EV signaling in the airway through the incorporation of primary cells.

STAR★METHODS

Detailed methods are provided in the online version of this paper and include the following:

- KEY RESOURCES TABLE
- RESOURCE AVAILABILITY
  - Lead contact
  - Materials availability
  - Data and code availability

SUPPLEMENTAL INFORMATION

Supplemental information can be found online at https://doi.org/10.1016/j.isci.2023.108162.

ACKNOWLEDGMENTS

The authors would like to thank UNC core facilities for their contributions to this project, including the UNC Nanomedicines Characterization Core Facility within the Eshelman School of Pharmacy (including Marina Sokolsky), the UNC Proteomics Core Facility within the School of Medicine (including Natalie Barker), and the UNC Microscopy Services Laboratory within the School of Medicine (including Kristen White). The research described in this manuscript has been reviewed by the Center for Public Health and Environmental Assessment, U.S. EPA, and approved for publication. Approval does not signify that contents necessarily reflect the views and policies of the agency, nor does the mention of trade names or commercial products constitute endorsement or recommendation for use. Funding: This study was supported by grants from the National Institutes of Health (NIH) from the National Institute of Environmental Health Sciences (1R21ES031740, P42ES031007, T32ES007018) and the Intramural Research Program of the U.S. Environmental Protection Agency's Office of Research and Development. Additional support was provided by the Institute for Environmental Health Solutions (IEHS) at the UNC Gillings School of Global Public Health and the Center for Environmental Medicine, Asthma and Lung Biology (CEMALB) at the UNC School of Medicine through a cooperative agreement (CR84033801). This study is based in part upon work conducted using the UNC Proteomics Core Facility, which is supported in part by P30 CA016086 Cancer Center Core Support Grant to the UNC Lineberger Comprehensive Cancer Center.

AUTHOR CONTRIBUTIONS

Conceptualization: ECMV, SDM, JER; Methodology: ECMV, CKC, AP, LEH, ALM, SDM, JER; Data Curation: ECMV, CKC, AP, LEH, ALM, SDM, JER; Writing–original draft: ECMV, CKC, SDM, JER; Writing–revisions and editing: ECMV, CKC, SDM, JER; Writing–final approval: ECMV, CKC, AP, LEH, ALM, SDM, JER.

DECLARATION OF INTERESTS

The authors declare that they have no competing interests.

INCLUSION AND DIVERSITY

We support inclusive, diverse, and equitable conduct of research.

Received: May 2, 2023
Revised: September 1, 2023
Accepted: October 5, 2023
Published: October 10, 2023

REFERENCES

1. Carberry, C.K., Keshava, D., Payton, A., Smith, G.J., and Rager, J.E. (2022). Approaches to incorporate extracellular vesicles into exposure science, toxicology, and public health research. J. Expo. Sci. Environ. Epidemiol. *32*, 647–659. https://doi.org/10.1038/s41370-022-00417-w.

2. Chuo, S.T.Y., Chien, J.C.Y., and Lai, C.P.K. (2018). Imaging extracellular vesicles: current and emerging methods. J. Biomed. Sci. *25*, 91. https://doi.org/10.1186/s12929-018-0494-5.

3. Doyle, L.M., and Wang, M.Z. (2019). Overview of Extracellular Vesicles, Their Origin, Composition, Purpose, and Methods for

Exosome Isolation and Analysis. Cells *8*. https://doi.org/10.3390/cells8070727.

4. Esquivel-Ruiz, S., González-Rodríguez, P., Lorente, J.A., Pérez-Vizcaíno, F., Herrero, R., and Moreno, L. (2021). Extracellular Vesicles and Alveolar Epithelial-Capillary Barrier Disruption in Acute Respiratory Distress Syndrome: Pathophysiological Role and Therapeutic Potential. Front. Physiol. *12*, 752287. https://doi.org/10.3389/fphys.2021.752287.
5. Carberry, C.K., Koval, L.E., Payton, A., Hartwell, H., Ho Kim, Y., Smith, G.J., Reif, D.M., Jaspers, I., Ian Gilmour, M., and Rager, J.E. (2022). Wildfires and extracellular vesicles: Exosomal MicroRNAs as mediators of cross-tissue cardiopulmonary responses to biomass smoke. Environ. Int. *167*, 107419. https://doi.org/10.1016/j.envint.2022.107419.
6. Chen, H., Samet, J.M., Bromberg, P.A., and Tong, H. (2021). Cardiovascular health impacts of wildfire smoke exposure. Part. Fibre Toxicol. *18*, 2. https://doi.org/10.1186/s12989-020-00394-8.
7. Chen, H., Xu, Y., Rappold, A., Diaz-Sanchez, D., and Tong, H. (2020). Effects of ambient ozone exposure on circulating extracellular vehicle microRNA levels in coronary artery disease patients. J. Toxicol. Environ. Health *83*, 351–362. https://doi.org/10.1080/15287394.2020.1762814.
8. Guervilly, C., Lacroix, R., Forel, J.M., Roch, A., Camoin-Jau, L., Papazian, L., and Dignat-George, F. (2011). High levels of circulating leukocyte microparticles are associated with better outcome in acute respiratory distress syndrome. Crit. Care *15*, R31. https://doi.org/10.1186/cc9978.
9. Lee, H., Zhang, D., Laskin, D.L., and Jin, Y. (2018). Functional Evidence of Pulmonary Extracellular Vesicles in Infectious and Noninfectious Lung Inflammation. J. Immunol. *201*, 1500–1509. https://doi.org/10.4049/jimmunol.1800264.
10. Pastor, L., Vera, E., Marin, J.M., and Sanz-Rubio, D. (2021). Extracellular Vesicles from Airway Secretions: New Insights in Lung Diseases. Int. J. Mol. Sci. *22*, 583. https://doi.org/10.3390/ijms22020583.
11. Shikano, S., Gon, Y., Maruoka, S., Shimizu, T., Kozu, Y., Iida, Y., Hikichi, M., Takahashi, M., Okamoto, S., Tsuya, K., et al. (2019). Increased extracellular vesicle miRNA-466 family in the bronchoalveolar lavage fluid as a precipitating factor of ARDS. BMC Pulm. Med. *19*, 110. https://doi.org/10.1186/s12890-019-0876-9.
12. Bowers, E.C., Hassanin, A.A.I., and Ramos, K.S. (2020). In vitro models of exosome biology and toxicology: New frontiers in biomedical research. Toxicol. Vitro *64*, 104462. https://doi.org/10.1016/j.tiv.2019.02.016.
13. Fujita, Y., Araya, J., Ito, S., Kobayashi, K., Kosaka, N., Yoshioka, Y., Kadota, T., Hara, H., Kuwano, K., and Ochiya, T. (2015). Suppression of autophagy by extracellular vesicles promotes myofibroblast differentiation in COPD pathogenesis. J. Extracell. Vesicles *4*, 28388. https://doi.org/10.3402/jev.v4.28388.
14. Guervilly, C., Bonifay, A., Burtey, S., Sabatier, F., Cauchois, R., Abdili, E., Arnaud, L., Lano, G., Pietri, L., Robert, T., et al. (2021). Dissemination of extreme levels of extracellular vesicles: tissue factor activity in patients with severe COVID-19. Blood Adv. *5*, 628–634. https://doi.org/10.1182/bloodadvances.2020003308.
15. Makiguchi, T., Yamada, M., Yoshioka, Y., Sugiura, H., Koarai, A., Chiba, S., Fujino, N., Tojo, Y., Ota, C., Kubo, H., et al. (2016). Serum extracellular vesicular miR-21-5p is a predictor of the prognosis in idiopathic pulmonary fibrosis. Respir. Res. *17*, 110. https://doi.org/10.1186/s12931-016-0427-3.
16. Martin-Medina, A., Lehmann, M., Burgy, O., Hermann, S., Baarsma, H.A., Wagner, D.E., De Santis, M.M., Ciolek, F., Hofer, T.P., Frankenberger, M., et al. (2018). Increased Extracellular Vesicles Mediate WNT5A Signaling in Idiopathic Pulmonary Fibrosis. Am. J. Respir. Crit. Care Med. *198*, 1527–1538. https://doi.org/10.1164/rccm.201708-1580OC.
17. Xu, H., Ling, M., Xue, J., Dai, X., Sun, Q., Chen, C., Liu, Y., Zhou, L., Liu, J., Luo, F., et al. (2018). Exosomal microRNA-21 derived from bronchial epithelial cells is involved in aberrant epithelium-fibroblast cross-talk in COPD induced by cigarette smoking. Theranostics *8*, 5419–5433. https://doi.org/10.7150/thno.27876.
18. He, S., Gui, J., Xiong, K., Chen, M., Gao, H., and Fu, Y. (2022). A roadmap to pulmonary delivery strategies for the treatment of infectious lung diseases. J. Nanobiotechnology *20*, 101. https://doi.org/10.1186/s12951-022-01307-x.
19. Bartel, S., Deshane, J., Wilkinson, T., and Gabrielsson, S. (2020). Extracellular Vesicles as Mediators of Cellular Cross Talk in the Lung Microenvironment. Front. Med. *7*, 326. https://doi.org/10.3389/fmed.2020.00326.
20. Thippabhotla, S., Zhong, C., and He, M. (2019). 3D cell culture stimulates the secretion of in vivo like extracellular vesicles. Sci. Rep. *9*, 13012. https://doi.org/10.1038/s41598-019-49671-3.
21. Ural, E.E., Toomajian, V., Hoque Apu, E., Veletic, M., Balasingham, I., Ashammakhi, N., Kanada, M., and Contag, C.H. (2021). Visualizing Extracellular Vesicles and Their Function in 3D Tumor Microenvironment Models. Int. J. Mol. Sci. *22*, 4784. https://doi.org/10.3390/ijms22094784.
22. Villasante, A., Marturano-Kruik, A., Ambati, S.R., Liu, Z., Godier-Furnemont, A., Parsa, H., Lee, B.W., Moore, M.A.S., and Vunjak-Novakovic, G. (2016). Recapitulating the Size and Cargo of Tumor Exosomes in a Tissue-Engineered Model. Theranostics *6*, 1119–1130. https://doi.org/10.7150/thno.13944.
23. Baarsma, H.A., Skronska-Wasek, W., Mutze, K., Ciolek, F., Wagner, D.E., John-Schuster, G., Heinzelmann, K., Günther, A., Bracke, K.R., Dagouassat, M., et al. (2017). Correction: Noncanonical WNT-5A signaling impairs endogenous lung repair in COPD. J. Exp. Med. *214*, 565. https://doi.org/10.1084/jem.2016067501052017c.
24. Wang, Z.N., and Tang, X.X. (2020). New Perspectives on the Aberrant Alveolar Repair of Idiopathic Pulmonary Fibrosis. Front. Cell Dev. Biol. *8*, 580026. https://doi.org/10.3389/fcell.2020.580026.
25. Kramer, A.A., Postler, G., Salhab, K.F., Mendez, C., Carey, L.C., and Rabb, H. (1999). Renal ischemia/reperfusion leads to macrophage-mediated increase in pulmonary vascular permeability. Kidney Int. *55*, 2362–2367. https://doi.org/10.1046/j.1523-1755.1999.00460.x.
26. London, N.R., Zhu, W., Bozza, F.A., Smith, M.C.P., Greif, D.M., Sorensen, L.K., Chen, L., Kaminoh, Y., Chan, A.C., Passi, S.F., et al. (2010). Targeting Robo4-dependent Slit signaling to survive the cytokine storm in sepsis and influenza. Sci. Transl. Med. *2*, 23ra19. https://doi.org/10.1126/scitranslmed.3000678.
27. Faber, S.C., McNabb, N.A., Ariel, P., Aungst, E.R., and McCullough, S.D. (2020). Exposure Effects Beyond the Epithelial Barrier: Transepithelial Induction of Oxidative Stress by Diesel Exhaust Particulates in Lung Fibroblasts in an Organotypic Human Airway Model. Toxicol. Sci. *177*, 140–155. https://doi.org/10.1093/toxsci/kfaa085.
28. Deregibus, M.C., Figliolini, F., D'Antico, S., Manzini, P.M., Pasquino, C., De Lena, M., Tetta, C., Brizzi, M.F., and Camussi, G. (2016). Charge-based precipitation of extracellular vesicles. Int. J. Mol. Med. *38*, 1359–1366. https://doi.org/10.3892/ijmm.2016.2759.
29. Kesimer, M., and Gupta, R. (2015). Physical characterization and profiling of airway epithelial derived exosomes using light scattering. Methods *87*, 59–63. https://doi.org/10.1016/j.ymeth.2015.03.013.
30. Wang, Y., Zhang, L., Li, Y., Chen, L., Wang, X., Guo, W., Zhang, X., Qin, G., He, S.H., Zimmerman, A., et al. (2015). Exosomes/microvesicles from induced pluripotent stem cells deliver cardioprotective miRNAs and prevent cardiomyocyte apoptosis in the ischemic myocardium. Int. J. Cardiol. *192*, 61–69. https://doi.org/10.1016/j.ijcard.2015.05.020.
31. Bachurski, D., Schuldner, M., Nguyen, P.H., Malz, A., Reiners, K.S., Grenzi, P.C., Babatz, F., Schauss, A.C., Hansen, H.P., Hallek, M., and Pogge von Strandmann, E. (2019). Extracellular vesicle measurements with nanoparticle tracking analysis - An accuracy and repeatability comparison between NanoSight NS300 and ZetaView. J. Extracell. Vesicles *8*, 1596016. https://doi.org/10.1080/20013078.2019.1596016.
32. Théry, C., Witwer, K.W., Aikawa, E., Alcaraz, M.J., Anderson, J.D., Andriantsitohaina, R., Antoniou, A., Arab, T., Archer, F., Atkin-Smith, G.K., et al. (2018). Minimal information for studies of extracellular vesicles 2018 (MISEV2018): a position statement of the International Society for Extracellular Vesicles and update of the MISEV2014 guidelines. J. Extracell. Vesicles *7*, 1535750. https://doi.org/10.1080/20013078.2018.1535750.
33. Ren, H., Birch, N.P., and Suresh, V. (2016). An Optimised Human Cell Culture Model for Alveolar Epithelial Transport. PLoS One *11*, e0165225. https://doi.org/10.1371/journal.pone.0165225.
34. Salomon, J.J., Muchitsch, V.E., Gausterer, J.C., Schwagerus, E., Huwer, H., Daum, N., Lehr, C.M., and Ehrhardt, C. (2014). The cell line NCI-H441 is a useful in vitro model for transport studies of human distal lung epithelial barrier. Mol. Pharm. *11*, 995–1006. https://doi.org/10.1021/mp4006535.
35. Bourdonnay, E., Zasłona, Z., Penke, L.R.K., Speth, J.M., Schneider, D.J., Przybranowski, S., Swanson, J.A., Mancuso, P., Freeman, C.M., Curtis, J.L., and Peters-Golden, M. (2015). Transcellular delivery of vesicular SOCS proteins from macrophages to epithelial cells blunts inflammatory signaling. J. Exp. Med. *212*, 729–742. https://doi.org/10.1084/jem.20141675.
36. Esser, J., Gehrmann, U., D'Alexandri, F.L., Hidalgo-Estévez, A.M., Wheelock, C.E., Scheynius, A., Gabrielsson, S., and Rådmark, O. (2010). Exosomes from human macrophages and dendritic cells contain

enzymes for leukotriene biosynthesis and promote granulocyte migration. J. Allergy Clin. Immunol. *126*, 1032–1040. 1040.e1-4. https://doi.org/10.1016/j.jaci.2010.06.039.

37. Lacy, S.H., Woeller, C.F., Thatcher, T.H., Pollock, S.J., Small, E.M., Sime, P.J., and Phipps, R.P. (2019). Activated Human Lung Fibroblasts Produce Extracellular Vesicles with Antifibrotic Prostaglandins. Am. J. Respir. Cell Mol. Biol. *60*, 269–278. https://doi.org/10.1165/rcmb.2017-0248OC.
38. Maacha, S., Bhat, A.A., Jimenez, L., Raza, A., Haris, M., Uddin, S., and Grivel, J.C. (2019). Extracellular vesicles-mediated intercellular communication: roles in the tumor microenvironment and anti-cancer drug resistance. Mol. Cancer *18*, 55. https://doi.org/10.1186/s12943-019-0965-7.
39. Sha, Z., Brill, L.M., Cabrera, R., Kleifeld, O., Scheliga, J.S., Glickman, M.H., Chang, E.C., and Wolf, D.A. (2009). The eIF3 interactome reveals the translasome, a supercomplex linking protein synthesis and degradation machineries. Mol. Cell *36*, 141–152. https://doi.org/10.1016/j.molcel.2009.09.026.
40. Cnop, M., Toivonen, S., Igoillo-Esteve, M., and Salpea, P. (2017). Endoplasmic reticulum stress and eIF2alpha phosphorylation: The Achilles heel of pancreatic beta cells. Mol. Metab. *6*, 1024–1039. https://doi.org/10.1016/j.molmet.2017.06.001.
41. Emanuelli, G., Nassehzadeh-Tabriz, N., Morrell, N.W., and Marciniak, S.J. (2020). The integrated stress response in pulmonary disease. Eur. Respir. Rev. *29*, 200184. https://doi.org/10.1183/16000617.0184-2020.
42. Wek, R.C., Jiang, H.Y., and Anthony, T.G. (2006). Coping with stress: eIF2 kinases and translational control. Biochem. Soc. Trans. *34*, 7–11. https://doi.org/10.1042/BST20060007.
43. Wu, C.W., and Storey, K.B. (2021). mTOR Signaling in Metabolic Stress Adaptation. Biomolecules *11*, 681. https://doi.org/10.3390/biom11050681.
44. Dozio, V., and Sanchez, J.C. (2017). Characterisation of extracellular vesicle-subsets derived from brain endothelial cells and analysis of their protein cargo modulation after TNF exposure. J. Extracell. Vesicles *6*, 1302705. https://doi.org/10.1080/20013078.2017.1302705.
45. Ovchinnikova, L.A., Terekhov, S.S., Ziganshin, R.H., Bagrov, D.V., Filimonova, I.N., Zalevsky, A.O., and Lomakin, Y.A. (2021). Reprogramming Extracellular Vesicles for Protein Therapeutics Delivery. Pharmaceutics *13*, 768. https://doi.org/10.3390/pharmaceutics13060768.
46. Sork, H., Corso, G., Krjutskov, K., Johansson, H.J., Nordin, J.Z., Wiklander, O.P.B., Lee, Y.X.F., Westholm, J.O., Lehtiö, J., Wood, M.J.A., et al. (2018). Heterogeneity and interplay of the extracellular vesicle small RNA transcriptome and proteome. Sci. Rep. *8*, 10813. https://doi.org/10.1038/s41598-018-28485-9.
47. Yang, Z., Shi, J., Xie, J., Wang, Y., Sun, J., Liu, T., Zhao, Y., Zhao, X., Wang, X., Ma, Y., et al. (2020). Large-scale generation of functional mRNA-encapsulating exosomes via cellular nanoporation. Nat. Biomed. Eng. *4*, 69–83. https://doi.org/10.1038/s41551-019-0485-1.
48. Alvarez-Erviti, L., Seow, Y., Yin, H., Betts, C., Lakhal, S., and Wood, M.J.A. (2011). Delivery of siRNA to the mouse brain by systemic injection of targeted exosomes. Nat. Biotechnol. *29*, 341–345. https://doi.org/10.1038/nbt.1807.
49. Aslan, C., Kiaie, S.H., Zolbanin, N.M., Lotfinejad, P., Ramezani, R., Kashanchi, F., and Jafari, R. (2021). Exosomes for mRNA delivery: a novel biotherapeutic strategy with hurdles and hope. BMC Biotechnol. *21*, 20. https://doi.org/10.1186/s12896-021-00683-w.
50. Kojima, R., Bojar, D., Rizzi, G., Hamri, G.C.E., El-Baba, M.D., Saxena, P., Ausländer, S., Tan, K.R., and Fussenegger, M. (2018). Designer exosomes produced by implanted cells intracerebrally deliver therapeutic cargo for Parkinson's disease treatment. Nat. Commun. *9*, 1305. https://doi.org/10.1038/s41467-018-03733-8.
51. O'Brien, K., Breyne, K., Ughetto, S., Laurent, L.C., and Breakefield, X.O. (2020). RNA delivery by extracellular vesicles in mammalian cells and its applications. Nat. Rev. Mol. Cell Biol. *21*, 585–606. https://doi.org/10.1038/s41580-020-0251-y.
52. Mohan, A., Agarwal, S., Clauss, M., Britt, N.S., and Dhillon, N.K. (2020). Extracellular vesicles: novel communicators in lung diseases. Respir. Res. *21*, 175. https://doi.org/10.1186/s12931-020-01423-y.
53. Blair, L.A., Haven, A.K., and Bauer, N.N. (2016). Circulating microparticles in severe pulmonary arterial hypertension increase intercellular adhesion molecule-1 expression selectively in pulmonary artery endothelium. Respir. Res. *17*, 133. https://doi.org/10.1186/s12931-016-0445-1.
54. Letsiou, E., Sammani, S., Zhang, W., Zhou, T., Quijada, H., Moreno-Vinasco, L., Dudek, S.M., and Garcia, J.G.N. (2015). Pathologic mechanical stress and endotoxin exposure increases lung endothelial microparticle shedding. Am. J. Respir. Cell Mol. Biol. *52*, 193–204. https://doi.org/10.1165/rcmb.2013-0347OC.
55. Thomashow, M.A., Shimbo, D., Parikh, M.A., Hoffman, E.A., Vogel-Claussen, J., Hueper, K., Fu, J., Liu, C.Y., Bluemke, D.A., Ventetuolo, C.E., et al. (2013). Endothelial microparticles in mild chronic obstructive pulmonary disease and emphysema. The Multi-Ethnic Study of Atherosclerosis Chronic Obstructive Pulmonary Disease study. Am. J. Respir. Crit. Care Med. *188*, 60–68. https://doi.org/10.1164/rccm.201209-1697OC.
56. Califf, R.M. (2018). Biomarker definitions and their applications. Exp. Biol. Med. *243*, 213–221. https://doi.org/10.1177/1535370217750088.
57. Polverino, F., Celli, B.R., and Owen, C.A. (2018). COPD as an endothelial disorder: endothelial injury linking lesions in the lungs and other organs? (2017 Grover Conference Series). Pulm. Circ. *8*, 2045894018758528. https://doi.org/10.1177/2045894018758528.
58. Clancy, J.W., Sedgwick, A., Rosse, C., Muralidharan-Chari, V., Raposo, G., Method, M., Chavrier, P., and D'Souza-Schorey, C. (2015). Regulated delivery of molecular cargo to invasive tumour-derived microvesicles. Nat. Commun. *6*, 6919. https://doi.org/10.1038/ncomms7919.
59. Han, K.Y., Dugas-Ford, J., Seiki, M., Chang, J.H., and Azar, D.T. (2015). Evidence for the Involvement of MMP14 in MMP2 Processing and Recruitment in Exosomes of Corneal Fibroblasts. Invest. Ophthalmol. Vis. Sci. *56*, 5323–5329. https://doi.org/10.1167/iovs.14-14417.
60. Li, C.J., Liu, Y., Chen, Y., Yu, D., Williams, K.J., and Liu, M.L. (2013). Novel proteolytic microvesicles released from human macrophages after exposure to tobacco smoke. Am. J. Pathol. *182*, 1552–1562. https://doi.org/10.1016/j.ajpath.2013.01.035.
61. Shen, A.R., Zhong, X., Tang, T.T., Wang, C., Jing, J., Liu, B.C., and Lv, L.L. (2020). Integrin, Exosome and Kidney Disease. Front. Physiol. *11*, 627800. https://doi.org/10.3389/fphys.2020.627800.
62. Shimoda, M., and Khokha, R. (2017). Metalloproteinases in extracellular vesicles. Biochim. Biophys. Acta. Mol. Cell Res. *1864*, 1989–2000. https://doi.org/10.1016/j.bbamcr.2017.05.027.
63. Thuault, S., Ghossoub, R., David, G., and Zimmermann, P. (2022). A Journey on Extracellular Vesicles for Matrix Metalloproteinases: A Mechanistic Perspective. Front. Cell Dev. Biol. *10*, 886381. https://doi.org/10.3389/fcell.2022.886381.
64. Nolte, M.A., Nolte-'t Hoen, E.N.M., and Margadant, C. (2021). Integrins Control Vesicular Trafficking; New Tricks for Old Dogs. Trends Biochem. Sci. *46*, 124–137. https://doi.org/10.1016/j.tibs.2020.09.001.
65. European Bioinformatics Institute, E.-E. (2023). PRIDE (PRoteomics IDEntifications Database). https://www.ebi.ac.uk/pride/.
66. EV-TRACK Consortium, Van Deun, J., Mestdagh, P., Agostinis, P., Akay, Ö., Anand, S., Anckaert, J., Martinez, Z.A., Baetens, T., Beghein, E., et al. (2017). EV-TRACK: transparent reporting and centralizing knowledge in extracellular vesicle research. Nat. Methods *14*, 228–232. https://doi.org/10.1038/nmeth.4185.
67. CEMALB (2022). CEMALB-dataverse. https://dataverse.unc.edu/dataverse/cemalb.
68. CEMALB (2022). UNC-CEMALB/Characterizing-the-Extracellular-Vesicle-Proteomic-Landscape-of-the-Human-Airway-using-In-vitro-Orga. https://github.com/UNC-CEMALB/Characterizing-the-Extracellular-Vesicle-Proteomic-Landscape-of-the-Human-Airway-using-In-vitro-Orga.
69. McNabb, N.A., and McCullough, S.D. (2019). Collagen Coating for Tissue Culture. https://protocolexchange.researchsquare.com/article/pex-794/v2.
70. Vitucci, E., and McCullough, S.D. (2022). Culture of HULEC-5a Cells. Protocol Exchange. https://protocolexchange.researchsquare.com/.
71. Vitucci, E., and McCullough, S.D. (2022). Culture of IMR90 Cells in Advanced RPMI. Protocol Exchange. https://protocolexchange.researchsquare.com/.
72. Vitucci, E., and McCullough, S.D. (2022). Culture of NCI-H441 Cells in Advanced RPMI. Protocol Exchange. https://protocolexchange.researchsquare.com/.
73. Vitucci, E., and McCullough, S.D. (2022). Alveolar Capillary Region Exposure (ACRE) Model. Protocol Exchange. https://protocolexchange.researchsquare.com/.
74. UniProt. (2022). Proteomics - Homo sapiens (Human). https://www.uniprot.org/proteomes/UP000005640.
75. ThermoScientific. (2017). Proteome Discoverer User Guide, Software Version 2.2. https://assets.thermofisher.com/TFS-Assets/CMD/manuals/Man-XCALI-97808-Proteome-Discoverer-User-ManXCALI97808-EN.pdf.
76. RDocumentation. (2022). impute.QRILC: Imputation of Left-Censored Missing Data Using QRILC Method. https://www.rdocumentation.org/packages/imputeLCMD/versions/2.0/topics/impute.QRILC.
77. Wei, R., Wang, J., Su, M., Jia, E., Chen, S., Chen, T., and Ni, Y. (2018). Missing Value

Imputation Approach for Mass Spectrometry-based Metabolomics Data. Sci. Rep. *8*, 663. https://doi.org/10.1038/s41598-017-19120-0.

78. RDocumentation. (2022). Prcomp: Principal Components Analysis. https://www.rdocumentation.org/packages/stats/versions/3.6.2/topics/prcomp.

79. Qiagen. (2022). QIAGEN Ingenuity Pathway Analysis (QIAGEN IPA). https://digitalinsights.qiagen.com/products-overview/discovery-insights-portfolio/analysis-and-visualization/qiagen-ipa/.

80. (2022). Gene Ontology. http://geneontology.org/.

81. Klaren, W.D., Ring, C., Harris, M.A., Thompson, C.M., Borghoff, S., Sipes, N.S., Hsieh, J.H., Auerbach, S.S., and Rager, J.E. (2019). Identifying Attributes That Influence In Vitro-to-In Vivo Concordance by Comparing In Vitro Tox21 Bioactivity Versus In Vivo DrugMatrix Transcriptomic Responses Across 130 Chemicals. Toxicol. Sci. *167*, 157–171. https://doi.org/10.1093/toxsci/kfy220.

82. Ring, C., Sipes, N.S., Hsieh, J.H., Carberry, C., Koval, L.E., Klaren, W.D., Harris, M.A., Auerbach, S.S., and Rager, J.E. (2021). Predictive modeling of biological responses in the rat liver using in vitro Tox21 bioactivity: Benefits from high-throughput toxicokinetics. Comput. Toxicol. *18*, 100166. https://doi.org/10.1016/j.comtox.2021.100166.

STAR★METHODS

KEY RESOURCES TABLE

REAGENT or RESOURCE	SOURCE	IDENTIFIER
Chemicals, peptides, and recombinant proteins		
Fluorescein isothiocyanate (FITC)	Sigma	Cat#F6377
Tetramethylrhodamine (TRITC) -labeled 4 kDa dextran	Sigma	Cat#T1037
Critical commercial assays		
LIVE/DEAD™ Cell Imaging Kit (488/570)	ThermoFisher	Cat#R37601
Exosome Isolation (from media) kit	ThermoFisher	Cat#4478359
Exo-Check antibody array	System Biosciences	Cat#EXORAY210B-8
Pierce™ BCA Protein Assay Kit	Thermo Scientific	Cat#23225
WesternBright Sirius HRP substrate	Advansta	Cat#K-12043-D10
Deposited data		
EV isolation methods and study logistics	This paper	EV-Track knowledgebase (EV-TRACK ID: EV230971)
Cell viability, cell permeability, NTA, and proteomics data	This paper	UNC Center for Environmental Medicine, Asthma and Lung Biology (UNC-CEMALB)-Dataverse (https://dataverse.unc.edu/dataverse/cemalb)
Script used to analyze NTA and proteomics data	This paper	UNC-CEMALB Github website (https://github.com/UNC-CEMALB/Characterizing-the-Extracellular-Vesicle-Proteomic-Landscape-of-the-Human-Airway-using-In-vitro-Orga)
full proteomics mass spectrometry data	This paper	PRoteomics IDEntifications Database (PRIDE Project accession: PXD040470)
Experimental models: Cell lines		
NCI-H441 cells	American Tissue Cell Collection [ATCC]	Cat#CRM-HTB-174, Batch #F-14929
IMR90 cells (human lung fibroblasts	American Tissue Cell Collection [ATCC]	Cat#CCL-182, Batch #64155514
HULEC-5a cells	American Tissue Cell Collection [ATCC]	Cat#CRL-3244, Batch #70025430
Software and algorithms		
Proteome Discoverer	Thermo Scientific, version 2.5	N/A
Ingenuity Pathway Analysis	Qiagen	N/A
Gene Ontology (GO) analysis	Protein ANalysis THrough Evolutionary Relationships (PANTHER) 17.0 database	https://geneontology.org/

RESOURCE AVAILABILITY

Lead contact

Requests for further information, resources, and reagents should be directed to and will be fulfilled by the lead contact, Julia Rager (jrager@unc.edu).

Materials availability

This study did not generate new unique reagents.

Data and code availability

- The full proteomics mass spectrometry data were uploaded into the PRoteomics IDEntifications Database (PRIDE) and are publicly available as of the date of publication.[65] EV isolation methods and study logistics have been uploaded to the EV-Track knowledgebase

(EV-TRACK ID: EV230971).[66] Cell viability, cell permeability, NTA, and proteomics data were also uploaded to the UNC Center for Environmental Medicine, Asthma and Lung Biology (UNC-CEMALB)-Dataverse.[67] The PRIDE project accession number, EV-TRACK ID, and accession link to UNC-CEMALB-Dataverse are listed in the key resources table.

- Script used to analyze NTA and proteomics data were organized via the UNC-CEMALB Github website and is publicly available as of the date of publication.[68]
- Any additional information required to reanalyze the data reported in this paper is available from the lead contact upon request.

EXPERIMENTAL MODEL AND STUDY PARTICIPANT DETAILS

Cell culture

All cell types were maintained in a humidified cell culture incubator at 37°C with 5% CO_2 and ambient O_2 levels (hereafter referred to as a "tissue culture incubator"). All cells were passaged onto tissue culture dishes (Techno Plastic Products, #93150 and 93100) coated with bovine type I collagen solution (Advanced BioMatrix, San Diego, CA, #5005).[69] All cell types were authenticated by short tandem repeat (STR) profiling using the ATCC Human Cell Authentication Service (ATCC #135-XV; results included in supplemental information) and tested negative for *Mycoplasma* spp. contamination (Universal Mycoplasma Detection Kit, ATCC #30-1012K).

The following three human cell types were selected to represent the alveolar capillary region of the lung: (1) alveolar epithelial cells, (2) fibroblasts, and (3) lung microvascular endothelial cells.

Alveolar epithelial cells:

NCI-H441 cells (hereafter referred to as "H441"; human, male, alveolar-like epithelial cells, American Tissue Cell Collection [ATCC] #CRM-HTB-174, Batch #F-14929) represented the alveolar epithelial cells and were obtained from the University of North Carolina (UNC)-Chapel Hill Tissue Culture Core Facility. This cell line was selected as it is the only human alveolar-like epithelial cell line that forms a functional, epithelial barrier (a critical function of the alveolar epithelium *in vivo*). H441 were used for *in vitro* airway culture model generation within an adjusted population doubling (APD) range of 4–27. Detailed cell culture methods for the H441 cell line is available through the online, publicly available Nature Portfolio, Protocol Exchange.[69–72] In brief, IMR90 were maintained in Advanced-RPMI growth medium (A-RPMI; ThermoFisher #12633020) supplemented with 5% FBS (ThermoFisher, #16000044, certified), 0.5% Penicillin/Streptomycin (P/S; ThermoFisher, #15140122) and 4 mM GlutaMAX (ThermoFisher #35050061)).

Fibroblasts:

IMR90 cells (human, female, lung fibroblasts; ATCC #CCL-182, Batch #64155514) represented the fibroblasts and were obtained from ATCC. This cell line was selected as it is a human lung fibroblast line and grows well with the other cell types of the organotypic models. IMR90 were used for *in vitro* airway culture model generation within an adjusted population doubling (APD) range of 3–15. Detailed cell culture methods for the IMR90 cell line is available through the online, publicly available Nature Portfolio, Protocol Exchange.[69–72] In brief, IMR90 were maintained in Advanced-RPMI growth medium (A-RPMI; ThermoFisher #12633020) supplemented with 5% FBS (ThermoFisher, #16000044, certified), 0.5% Penicillin/Streptomycin (P/S; ThermoFisher, #15140122) and 4 mM GlutaMAX (ThermoFisher #35050061)).

Lung microvascular endothelial cells:

HULEC-5a cells (hereafter referred to as "HULEC"; human, male, lung microvascular endothelial cells, ATCC #CRL-3244, Batch #70025430) represented the endothelial cells and were obtained from ATCC. This cell line was selected as it is one of the only human lung microvascular endothelial cell lines available that can be expanded in culture similar to other immortalized cell lines. HULEC were used for *in vitro* airway culture model generation within an adjusted population doubling (APD) range of 3–12. Detailed cell culture methods for the HULEC-5a cell line is available through the online, publicly available Nature Portfolio, Protocol Exchange.[69–72] HULEC were maintained in complete HULEC growth medium (MCDB-131 (Gibco #10372019) supplemented with 10% FBS, 1% P/S, 10 mM GlutaMAX, 10 ng/mL human Epidermal Growth Factor (Fisher Scientific, #PHG0311), and 1μg/mL hydrocortisone (MilliporeSigma, #H0888)).

METHOD DETAILS

Tri- and co-culture model setup

The tri-culture and co-culture models were setup following the "Alveolar Capillary Region Exposure (ACRE) Exposure Model" methodology, detailed in full through the online, publicly available Nature Portfolio, Protocol Exchange[73] up to Day 3. On day 3 of the tri-culture model setup, HULECs were seeded in separate collagen-coated[69] multi-well plates in complete HULEC growth medium and incubated in a tissue culture incubator for 9 h to permit the formation of a confluent monolayer. After the 9 h incubation period, the medium was aspirated and replaced with HULEC Exposure Medium (MCDB-131 supplemented with 1% exosome-depleted FBS (Gibco #A2720803), 1% P/S, and 10mM GlutaMAX). In contrast, for the co-culture model setup, cell-free HULEC Exposure Medium was plated in separate multi-well plates to imitate a HULEC plating event. The apical and basolateral media from the seeded Transwell inserts were aspirated from the inserts and the seeded inserts were carefully transferred to HULEC-seeded (tri-culture model) or HULEC-free (co-culture model) wells. Polarization medium (A-RPMI

growth medium supplemented with 0.5 μM dexamethasone (MilliporeSigma, #D4902)) was then added to the apical side of the Transwell inserts prior to the cultures being placed in a tissue culture incubator for 14 h. On day 4, the basolateral medium of the cultures was replaced with fresh HULEC Exposure Medium and the apical medium was replaced with Apical Exposure Medium (A-RPMI supplemented with 0.5% P/S, 0.5 μM dexamethasone, and 4mM GlutaMAX). The cultures were then incubated in a tissue culture incubator for 24 h. Following incubation, apical and basolateral compartments were separated for cell-specific functional analysis. Cell seeding densities, downstream applications, media volumes, and product numbers for the tri- and co-culture setup are summarized (Table 1). Culture models are also depicted (Figure 1).

Cell viability assay

Tri- and co-culture models were setup using the 12-well Transwell insert format described in Table 1. Cell viability of the tri- and co-culture models was assessed 24 h after the final medium change on day 4 of the model setups using the LIVE/DEAD™ Cell Imaging Kit (488/570) (ThermoFisher, #R37601). The apical medium of the *in vitro* models was aspirated from the seeded Transwell inserts and the basolateral medium was collected for downstream EV analysis. Following media removal and collection, the inserts were transferred to new multi-well plates. The seeded Transwell inserts and HULEC were rinsed with pre-warmed DPBS. A 2X-stock solution of the LIVE/DEAD reagents, 0.75 μl/mL Calcein AM and 1.5 μL/mL Ethidium homodimer-1, was prepared in DMEM-fluorobrite (DMEM-F; ThermoFisher, #A1896701) supplemented with 4mM GlutaMAX. This solution was then diluted two-fold in GlutaMAX supplemented DMEM-F and added to the apical and basolateral compartments of the seeded Transwell inserts and directly to the seeded HULEC cells. All cells were incubated in these LIVE/DEAD reagents for 40-min at room temperature. Cells were then analyzed at excitation/emission 488/515 nm (LIVE) and 570/602 nm (DEAD) on a CLARIOstar Plus plate reader (BMG LabTech, Cary, NC). Extra tri-culture model inserts were seeded for dead and live cell controls to obtain maximum DEAD signal and maximum LIVE signal from the seeded inserts and HULEC. Positive DEAD controls were generated according to the manufacturer's protocol. Positive LIVE controls were maintained in appropriate exposure medium. Values represent the mean (± SD) from three biological replicates (n = 3), which were each performed in technical triplicate, and normalized to their respective maximum DEAD and LIVE signal. Statistical analysis was conducted in GraphPad Prism (version 9.3.1). An ordinary two-way ANOVA and Šidák's multiple comparisons post-hoc test was run to investigate significant differences in cell viability between the seeded Transwell inserts of the tri- and co-culture models. An unpaired, two-tailed t-test between the LIVE and DEAD signal from the HULEC in the tri-culture was also run to investigate HULEC viability in the tri-culture model.

Small molecule permeability assay

Similar to the cell viability assessment, additional replicates of the tri- and co-culture models were setup using the 12-well Transwell insert format described in Table 1. Small molecule permeability across the tri- and co-culture seeded Transwell inserts was investigated 24 h after the final medium change on day 4 of the model setups. The apical medium of the *in vitro* models was aspirated from the seeded Transwell inserts and the basolateral medium was collected for downstream EV analysis. Following the medium removal and collection, the seeded inserts of the tri- and co-culture models were rinsed with pre-warmed DPBS and transferred to new multi-well plates. Pre-warmed basal DMEM-F was added to the basolateral compartment of each well. A 1 mg/mL suspension of fluorescein isothiocyanate (FITC, Sigma, #F6377) and a 1 mg/mL suspension of Tetramethylrhodamine (TRITC) -labeled 4 kDa dextran, (Sigma, #T1037) were mixed at a 1:1 ratio in basal DMEM-F and were added to the apical compartment of the DPBS-washed seeded Transwell inserts. These inserts were incubated in the presence of the FITC/TRITC solution for 20 min in a tissue culture incubator and protected from light. After incubation, the basolateral medium was collected from each well, vortexed and 100 μL of each well's basolateral medium was transferred into wells of black 96-well plates (Corning, #3603) in triplicate. Samples collected from unseeded, non-collagen coated inserts were collected and plated in the same black 96-well plates to determine maximum small molecule permeability of the Transwell inserts. Average fluorescence at 490/520 nm (excitation/emission maxima) across all technical triplicate wells was measured using a CLARIOstar Plus plate reader (BMG LabTech, Cary, NC). Small molecule permeability of independent experiments was determined by averaging the fluorescence intensity of the basolateral medium from three inserts (technical triplicates within an independent experiment), expressed as a percentage of the maximum small molecule permeability observed in each experiment. The data shown represent the mean (± SD) of five biological replicates (n = 5). Statistical analysis was conducted in GraphPad Prism (version 9.3.1) using an unpaired, two-tailed t-test between the tri- and co-culture samples.

Conditioned media processing and isolation of exosome-enriched EVs

To investigate EV characteristics and proteomic changes between the tri- and co-culture models, the basolateral conditioned medium was collected from each well of the 12-well Transwell inserts designated for the cell viability and small molecular permeability assay as described above. 24 h after the final media change on day 4 of the model setup, basolateral conditioned medium was also collected from additional tri- and co-culture models seeded using the 6-well Transwell insert format described in Table 1. For all conditioned medium collected, cell debris were removed via centrifugation (13,000 × *g* for 10 minutes at 4°C). Notably, it is possible that pre-processing steps may have caused denser EVs such as apoptotic bodies or aggregates to sediment out prior to EV isolation. This centrifugation step was still carried out to meet the eventual goal of isolating smaller sized EVs that overlap with the targeted exosome size ranges. EVs were specifically isolated from conditioned medium using the Invitrogen Total Exosome Isolation (from media) kit (ThermoFisher, #4478359). The manufacturer's protocol was implemented with one additional spin at 10,000 × *g* for 30 min to enhance the removal of debris immediately prior to the addition of

precipitation reagent. Isolated EVs were resuspended in filtered PBS (200 μL and 50 μL for samples collected from 6- and 12-well formats, respectively). EV samples were validated and characterized using EV imaging, NTA, and proteomics analysis.

EV imaging

Two representative EV samples from the tri-culture model were imaged via negative stain transmission electron microscopy on different days during the study to ensure replicability. The sample was prepared by floating glow-discharged formvar/carbon-coated 400 mesh copper grids (Ted Pella, Inc, Redding, CA) onto droplets of sample aliquots (25 μL) for 10 minutes. Two drops of deionized water and one droplet of 2% aqueous uranyl acetate stain were then added to each grid for one minute. Grids were blotted with filter paper, air dried, and then visualized. Visualization was completed using a JEM-1230 transmission electron microscope (JEOL USA, Inc., Peabody, MA) operating at 80kV, and resulting images obtained using a Gatan Orius SC1000 CCD camera and associated Microscopy Suite software, v3.10.1002.0 (Gatan, Inc., Pleasanton, CA).

EV particle charge, count, and size characterization

NTA was used to characterize EV particle charge, count, and size distribution using a full set of n = 6 biological replicates per culture model from the 12-well design (Table 1). The Multiple–Laser ZetaView® f-NTA Nanoparticle Tracking Analyzers System (Particle Metrix, Mebane, NC) was run in scatter scanning mode to measure particle count and size distribution. Particle charge was measured via zeta-potential of particle mobility in an electric field. EV samples were diluted in filtered PBS at 1:1000 for particle count and size measures and 1:2000 for particle charge measures using 1.0 mL sample volumes. NTA data were organized and analyzed in R Software (v4.1.2), statistically evaluated for potential changes between culture models via the Wilcoxon Rank Sum test and visualized using ggplot2.

EV proteomics analysis

A full set of $n = 6$ EV biological replicates per culture model were analyzed for proteomic signatures through the UNC Proteomics Core Facility. Due to limited protein yields, four technical replicates were pooled using 1 mL aliquots from the 6-well design (Table 1). This approach ensured that technical replicates were prepared on the same day (and cell passage number), and thus still represented unique biological replicates once combined. Acetone (Thermo Scientific, #A18-4) protein precipitation was performed and protein pellets were reconstituted in 8M urea (Thermo Scientific, #29700). Samples were reduced with 5mM DTT (Pierce™, Thermo Scientific, #20290) for 30 min at 56C, alkylated with 15mM iodoacetamide (Thermo Scientific, #122270050) for 45 min at room temperature in the dark, then diluted to 1M urea with 50mM ammonium bicarbonate pH 7.8 (Sigma, #1066-33-7). Samples were digested with trypsin (Promega, #V5280) overnight at 37C. C18 desalting spin columns (Pierce™, Thermo Fisher Scientific, #89870) were used to clean resulting peptide samples, which were dried down via vacuum centrifugation and stored at −80C until further analysis.

Samples were analyzed by liquid chromatography coupled to tandem mass spectrometry (LC-MS/MS) using a Thermo Easy nLC 1200-QExactive HF. Samples were injected onto an Easy Spray PepMap C18 column (75 μm id × 25 cm, 2 μm particle size) (Thermo Scientific) and separated over a 120 min method. The gradient for separation consisted of a step gradient from 5 to 32 to 42% mobile phase B at a 250 nL/min flow rate, where mobile phase A was 0.1% formic acid in water and mobile phase B consisted of 0.1% formic acid in 80% ACN. The QExactive HF was operated in data-dependent mode where the 15 most intense precursors were selected for subsequent HCD fragmentation. Resolution for the precursor scan (m/z 375–1700) was set to 60,000 with a target value of 3×10^6 ions, 100ms inject time. MS/MS scans resolution was set to 15,000 with a target value of 1×10^5 ions, 100ms inject time. The normalized collision energy was set to 27% for HCD, with an isolation window of 1.6 m/z. Peptide match was set to preferred, and precursors with unknown charge or a charge state of 1 and ≥8 were excluded. Instrument variability was checked by including pooled samples, combined from equal volumes of all samples, and analyzing these before and after the sample run. Samples were randomized prior to LC-MS/MS, and all samples were analyzed consecutively minimizing the potential for batch effects.

EV proteomics data processing and statistical analysis

Proteins were identified and quantified using Proteome Discoverer (Thermo Scientific, version 2.5) with the UniProt Human database, containing ~20,000 proteins, appended with a common lab contaminants database used in general proteomic studies.[74] Further data processing and analysis was carried out in R Software (v4.1.2), where a series of pre-processing steps were applied to the initial set of 2,167 protein observations. Proteins abundances were normalized based on total peptide amount.[75] Non-detect proteins were treated as missing data and retained values of "NA" in this step. Second, a detection filter required that proteins were identified from at least two peptides. Third, a background filter was applied requiring that a protein be measured in at least 50% of the samples within either culture model (i.e., either detected in three of the six biological replicates of the co-culture and tri-culture groups). These filters yielded a list of 1,427 proteins (represented by 1,542 observed features) carried forward in the analysis.

Data were $\log_2$-transformed to allow for subsequent imputation and normalization algorithms. Missing data were imputed via quantile regression imputation of left-censored data (QRILC) through the imputeLCMD package, which replaces missing data with left-censored data from a Gaussian distribution.[76] This method was selected based on the assumption that data were missing not at random (MNAR) and likely represented proteins that were not present and/or below detection. Notably, QRILC has been shown to out-perform other imputation methods under conditions of MNAR.[77] Potential sample outliers were evaluated using principal component analysis (stats package).[78]

Resulting dimensionally reduced value distribution plots did not indicate samples with outlying distributions, and thus all biological samples were retained.

Statistical analyses then compared protein distributions in tri-culture vs. co-culture model samples using a t-test followed by a false discovery rate (FDR) adjustment for multiple testing, resulting in adjusted p values (P_{adj}). Fold change (FC) in expression was calculated as the ratio of the average abundance levels across tri-culture samples divided by the average abundance levels across co-culture samples, per protein. Following statistical analysis, contaminant proteins were excluded as identified through the UniProt contaminants database. 91 proteins (represented by 91 observations) were considered common lab contaminants (e.g., Bovine serum albumin). Following this exclusion, 1,336 proteins of biological interest remained (represented by 1,451 observations) and were detected in EVs in at least one culture model (Table S2). Global statistical results were visualized via volcano plots using GraphPad Prism (version 9.3.1).

After statistical analyses were completed, proteins were binned into the following categories based upon their distribution of expression changes[1]: 'Increased in tri-culture' – EV proteins that were loaded at increased levels in EVs from the tri-culture model (based off a $\log_2$FC (tri-culture/co-culture) ≥ 0.585), and that were significantly increased in the tri-culture/co-culture comparison (based off a $\log_2$FC ≥ 0.585 and $p_{adj} < 0.05$)[2]; 'Increased in co-culture' – EV proteins that were loaded at increased levels in EVs from the co-culture model (based off a $\log_2$FC (tri-culture/co-culture) ≤ -0.585, and that were significantly increased in the co-culture/tri-culture comparison (based off a $\log_2$FC ≤ -0.585 and $p_{adj} < 0.05$)[3]; 'No change' – the remaining proteins that were detected in either model but not increased in either model in comparison to the other.

Comparing detected EV proteins with markers of presence and purity

The International Society for Extracellular Vesicles (ISEV)'s Guidelines for Minimal Information for Studies of Extracellular Vesicles (MISEV) advocates for the measurement and reporting of certain proteins to characterize EVs used in research studies.[32] Important proteins highlighted by the ISEV include those that inform EV presence and purity, spanning the following categories[1] transmembrane or GPI-anchored proteins that inform the presence of an EV lipid bilayer[2]; cytosolic proteins present in eukaryotic cells that commonly incorporate into EVs[3]; proteins that often co-isolate with EVs and are thus considered contaminants. EV proteins detected in this study were compared against the MISEV's list of proteins in categories 1–3 that inform EV presence and purity.

Pathway and cellular compartment enrichment of EV proteins

To understand the biological implications of the measured EV proteins, pathway and cellular compartment enrichment analyses were carried out. For the pathway enrichment analysis, protein lists were evaluated using the Ingenuity Knowledge Database within Ingenuity Pathway Analysis (IPA; Qiagen).[79] Pathways that were considered significantly enriched were defined as pathways that were over-represented, containing more proteins than expected by random chance. For the compartment enrichment analysis, Gene Ontology (GO) analysis was carried out using the Protein ANalysis THrough Evolutionary Relationships (PANTHER) 17.0 database.[80] Cellular compartments or stable macromolecular complexes that were considered significantly enriched within each respective list of EV proteins were defined as over-represented cellular locations, with more proteins at these sites than expected by random chance (Table S4). The statistical filter applied for identification of over-represented pathways and cellular locations was $p < 0.01$, based off a Fisher's Exact Test with a Bonferroni multiple tests correction, paralleling methods and filters previously implemented in toxicological response comparisons.[81,82]

Protein-specific validation of EV isolates

Specific proteins were validated leveraging the System Bioscience Exo-Check antibody array (System Biosciences, #EXORAY210B-8), a semi-quantitative assay with pre-loaded antibodies printed on a membrane. This assay includes nine proteins commonly used in EV evaluations, including programmed cell death 6 interacting protein (ALIX), annexin A5 (ANXA5), tetraspanin 63 (CD63), tetraspanin 81 (CD81), epithelial cell adhesion molecule (EPCAM), flotillin 1 (FLOT1), cis-golgi matrix protein (GM130), intercellular adhesion molecule 1 (ICAM1), and tumor susceptibility gene 101 (TSG101). Protein was quantified for a subset of EV samples to estimate total EV protein using the Pierce™ BCA Protein Assay Kit (Thermo Scientific, #23225) with absorbance values read at 562 nm on a Molecular Devices SpectraMax iD5 Multi-Mode Microplate Reader. This assay required slightly higher amounts of protein in comparison to the proteomics screen, requiring the aggregation of EV samples isolated across five 1mL biological replicates from the 12-well tri-culture samples, resulting in the analysis of one collective EV sample from the tri-culture design. Antibody array measures were then collected according to manufacturer's protocol. A resulting membrane was developed using the WesternBright Sirius HRP substrate (Advansta, #K-12043-D10) and imaged using LI-COR Biosciences C-DiGit Blot Scanner and Image Studio software. Additionally, these nine proteins were evaluated within the EV proteomics data to verify their presence in or on EVs and visualized via GraphPad Prism (version 9.3.1).

QUANTIFICATION AND STATISTICAL ANALYSIS

Statistical analyses, as well as strategies for the randomization of samples for each experiment can be found in the STAR Methods section that describes the experiment. Significance was defined as $p < 0.05$.